


In Vivo Optogenetics Reveals Control of Cochlear Electromechanical Responses by Supporting Cells

Victoria A. Lukashkina,¹ Snezana Levic,^{1,3} Patrício Simões,¹ Zhenhang Xu,² Joseph A. DiGuseppi,² Jian Zuo,² Andrei N. Lukashin,¹ and  Ian J. Russell¹

¹Sensory Neuroscience Research Group, School of Applied Sciences, University of Brighton, Brighton, BN2 4GJ, United Kingdom, ²Department of Biomedical Sciences, Creighton University School of Medicine, Omaha, Nebraska 68178, and ³Brighton and Sussex Medical School, University of Sussex, Brighton, BN1 9PX, United Kingdom

Cochlear sensitivity, essential for communication and exploiting the acoustic environment, results from sensory-motor outer hair cells (OHCs) operating in a structural scaffold of supporting cells and extracellular cortilymph within the organ of Corti (OoC). Cochlear sensitivity control is hypothesized to involve interaction between the OHCs and OoC supporting cells (e.g., Deiters' cells [DCs] and outer pillar cells [OPCs]), but this has never been established *in vivo*. Here, we conditionally expressed channelrhodopsins (ChR2) specifically in male and female mouse DCs and OPCs. Illumination of the OoC activated the nonselective ChR2 cation conductance and depolarized DCs when measured *in vivo* and in isolated OoC. Measurements of sound-induced cochlear mechanical and electrical responses revealed that OoC illumination suppressed the normal functions of OoC supporting cells transiently and reversibly. OoC illumination blocked normally occurring continuous minor adjustments of tone-evoked basilar membrane displacements over their entire dynamic range and OHC voltage responses to tones at levels and frequencies subject to cochlear amplification. OoC illumination altered the OHC mechano-electrical transduction conductance operating point, which reversed the asymmetry of OHC voltage responses to high level tones. OoC illumination accelerated recovery from temporary loud sound-induced acoustic desensitization. We concluded that DCs and OPCs are involved in both the control of cochlear responses (which are essential for normal hearing) and the recovery from temporary acoustic desensitization. This is the first direct *in vivo* evidence for the interdependency of the structural, mechanical, and electrochemical arrangements of OHCs and OoC supporting cells that together provide fine control of cochlear responses.

Key words: cochlea; cochlear amplifier; cochlear supporting cells; optogenetics; organ of Corti; outer hair cells

Significance Statement

A striking feature of the mammalian cochlear sensory epithelium, the organ of Corti, is the cellular architecture and supporting cell arrangement that provides a structural scaffold for the sensory-motor outer hair cells. The role of the supporting cell scaffold, however, has never been elucidated *in vivo*, although *in vitro* and modeling studies indicate the scaffold is involved in exchange of forces between the outer hair cells and the organ of Corti. We used *in vivo* techniques, including optogenetics, that do not disrupt arrangements between the outer hair cells and supporting cells, but selectively, transiently, and reversibly interfere with supporting cell normal function. We revealed the supporting cells provide continuous adjustment of cochlear sensitivity, which is instrumental in normal hearing.

Received Oct. 25, 2021; revised Mar. 25, 2022; accepted Apr. 17, 2022.

Author contributions: I.J.R., J.Z., and A.N.L. designed research; I.J.R., V.A.L., S.L., P.S., Z.X., J.A.D., and A.N.L. performed research; I.J.R., V.A.L., S.L., P.S., J.Z., Z.X., J.A.D., and A.N.L. analyzed data; I.J.R. wrote the first draft of the paper; I.J.R., V.A.L., S.L., P.S., J.Z., and A.N.L. edited the paper; I.J.R. and A.N.L. wrote the paper.

This work was supported by Medical Research Council Grant MR/N004299/1. We thank Sarath Vijayakumar and Cassidy Nguyen for technical assistance on mouse colony management at Creighton University; and Milos Stankovic for assistance with Figure 1A.

The authors declare no competing financial interests.

P. Simões' present address: Sussex Neuroscience, School of Life Sciences, University of Sussex, Brighton BN1 9QG, United Kingdom.

Correspondence should be addressed to Ian J. Russell at I.Russell@brighton.ac.uk or Jian Zuo at JianZuo@creighton.edu.

<https://doi.org/10.1523/JNEUROSCI.2127-21.2022>

Copyright © 2022 the authors

Introduction

Cochlear outer hair cells (OHCs) (Ashmore, 2008; Dallos, 2008) interact with cellular and noncellular elements of the cochlear partition, including the basilar membrane (BM), reticular lamina (RL), and tectorial membrane (TM), via an enveloping cage of specialized supporting cells (see Fig. 1A,B), including outer pillar cells (OPCs) and Deiters' cells (DCs) (e.g., Nam, 2014; Motallebzadeh et al., 2018). Through this interaction, OHCs amplify responses to low-to-moderate-level sounds and compress responses to loud sounds over an enormous dynamic range. Simultaneously, OHC activity provides a basis for the

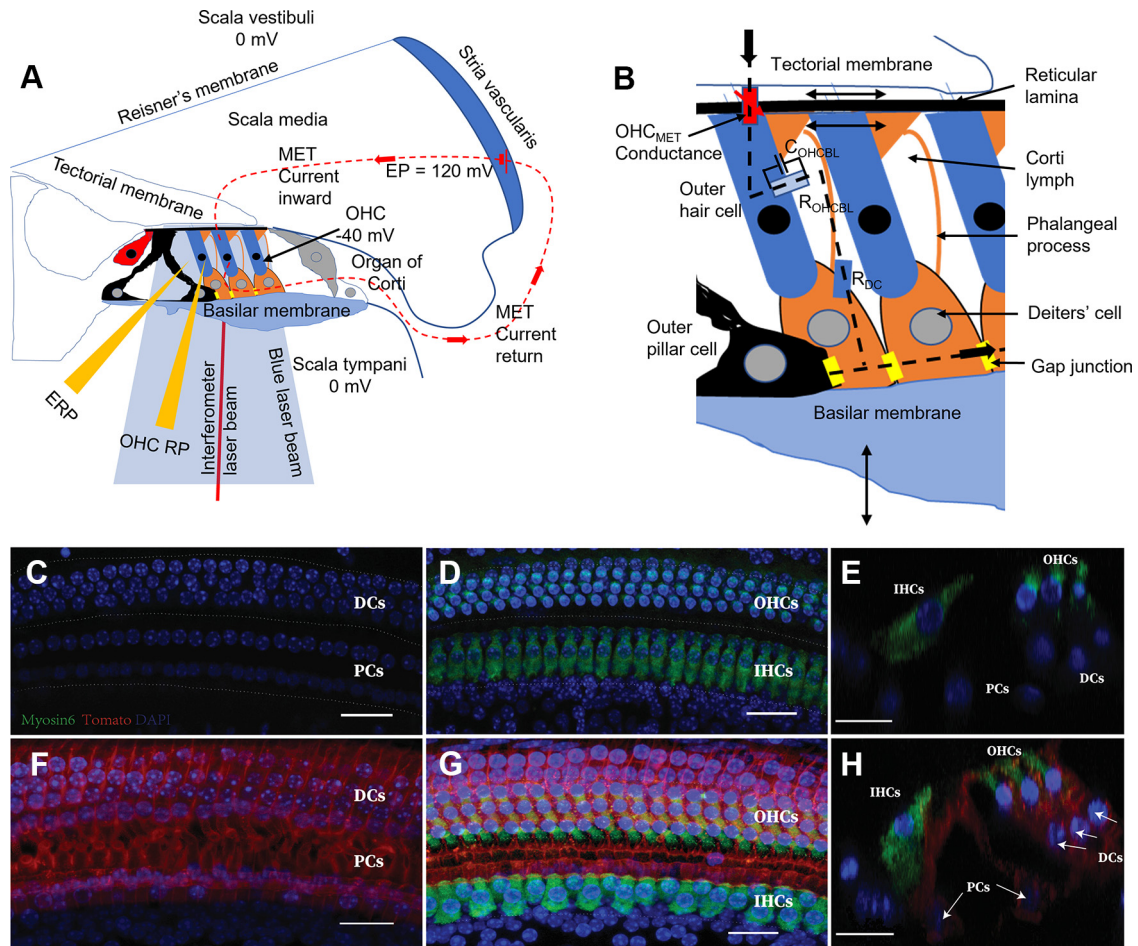


Figure 1. Schematic of the organ of Corti, *in vivo* physiological techniques, and expression of Chr2-tdTomato in its supporting cells. **A**, Schematic cross-section of inner ear, including OoC, with three fluid-filled chambers (scala tympani, scala media, and scala vestibuli) separated by the BM and Reisner's membrane. The positive endocochlear potential (EP) in series with the negative OHC membrane potential provides the battery driving the OoC, K^+ dominated, MET current pathway (**A,B**, dashed lines). OHC MET current is modulated when the OHC MET conductance (**B**, red lozenge) is modulated by OHC bundle displacement because of radial, shear displacements between the TM and the RL caused by transverse BM vibrations (arrows, **B**). K^+ exits OHCs down its electrochemical gradient through voltage-dependent K^+ conductance (light blue lozenge, **B**) to the CL, where it is taken up by K^+-Cl^- transporters in the DC lateral walls (blue lozenge) and through gap junctions (GJ; yellow lozenges) to the stria vascularis (**A,B**). **A**, Micropipettes recording potentials from the CL or scala media. A red self-mixing interferometer laser beam was used to measure BM displacements. The blue light beam activated Chr2 expressed in DCs and OPCs. **C–H**, Chr2 expression in the DCs and inner pillar cells and OPCs. *Fgfr3-iCreER^{T2}*; Chr2-tdTomato mice were induced with tamoxifen (TMX) at P12/P13 and analyzed at P28. **C–E**, *Fgfr3-iCreER^{T2}*; Chr2-tdTomato⁺ control mice. **F–H**, *Fgfr3-iCreER^{T2}*; Chr2-tdTomato⁺ experimental mice. **C, D, F, G**, Whole mounts of cochlear basal turns. **C, F**, Supporting-cell (SC) layers. **D, G**, Projections of SC and hair-cell (HC) layers. **E, H**, Optical cross-sections in **D, G**, respectively. Arrows indicate Chr2-tdTomato-expressing DCs and PCs. Green represents Myo6. Blue represents DAPI. Red represents tdTomato. Scale bar, 20 μ m.

precise frequency decomposition of complex sounds because of their tonotopic arrangement on the BM, which is graded in stiffness and frequency from the compliant low-frequency apex to the stiff, high-frequency base of the cochlea (Robles and Ruggero, 2001). Ultrastructural (Parsa et al., 2012), *in vitro* and *in vivo* electrophysiological, micromechanical (Zhu et al., 2013), and modeling studies (Nam, 2014; Motallebzadeh et al., 2018) support the concept that the structural scaffold of OPCs and DCs is critically located to transmit passive and active forces from OHCs to the structures of the cochlear partition. However, the role of the supporting cell cage has never been elucidated *in vivo*.

In addition to having a presumed role in the interactive transfer of forces between the major elements of the organ of Corti (OoC) and the OHCs, the DCs are also engaged in regulating the electrochemistry of the cortilymph (CL) (Santos-Sacchi, 1985; Hibino and Kurachi, 2006; Mistrik and Ashmore, 2009; Eckhard et al., 2012), which has potential consequences for mechano-electrical interaction between OHCs, DCs, and OPCs. During acoustic stimulation, when the OHC mechano-electrical transduction (MET)

channels located near the tips of the OHC hair-bundle stereocilia are gated (see Fig. 1A,B) (Corey and Hudspeth, 1979; Beurg et al., 2009), K^+ accumulates in the CL. This accumulation is because of the flow of K^+ down its electrochemical gradient, from the positive K^+ rich endolymph through the OHC MET channels, via the negative OHC resting membrane potential and K^+ conductance of the OHC basolateral membranes, to the Na^+ dominated CL (see Fig. 1A,B) (Davis, 1965; Russell, 1983; Wangemann, 2006). K^+ accumulation occurs in the CL even during moderate level sounds (Cody and Russell, 1988; Johnstone et al., 1989). Increased K^+ concentration in the CL, and simultaneous OHC depolarization, causes changes in OHC responses to acoustic stimulation (Cody and Russell, 1985, 1995), possibly through mechanical stimulation of the DCs, which affects OHC electromotility (Yu and Zhao, 2009). Preservation of the electrochemical state of the CL is therefore important for the metabolic state of the OHCs (Zdebik et al., 2009), sensory transduction, and cochlear amplification.

To test the hypothesis that DCs and OPCs have roles in controlling cochlear responses *in vivo*, we used optogenetic techniques that do not disrupt the structural arrangement

between the OHCs and supporting cells (Mellado Lagarde et al., 2014), but allow selective, transient, and reversible interference with the normal function of DCs and OPCs. The DCs and OPCs of optogenetic mice conditionally expressed a channelrodopsin, Chlamydomonas Opsin-tdTomato (ChR2) that, when light-activated, gates a large nonspecific cation conductance (Nagel et al., 2002, 2003) (see Materials and Methods; Fig. 1C–H). We measured BM mechanical responses, phasic extracellular receptor potentials (ERPs), and tonic ERPs (ERPDC) from the CL. We also measured cochlear desensitization following exposure to loud sounds in optogenetic mice with excellent high-frequency hearing. Activation of ChR2 expressed in DCs and OPCs, through OoC illumination, strongly and reversibly blocked the fine adjustments of cochlear mechanical and electrical responses and accelerated recovery of cochlear sensitivity from temporary noise-induced desensitization. The use of optogenetics to block an ongoing cochlear function provided an opportunity to examine the involvement of DCs and OPCs in controlling cochlear responses *in vivo*.

Materials and Methods

Mouse models and immunofluorescence

The Animal Resource Facilities of Creighton University approved protocols on mouse breeding, husbandry, and cochlear morphologic analysis performed in this study. All *in vitro* and *in vivo* experiments performed at the University of Brighton complied with Home Office guidelines under the Animals (Scientific Procedures) Act of 1986 and were approved by the University of Brighton Animal Welfare and Ethical Review Body.

Mice were housed in a facility with a 12 h light/dark cycle and free access to food and water. All mice used here were purchased from The Jackson Laboratory: *Fgfr3iCreER^{T2}* (stock #025809) and *Rosa-CAG-LSL-hChR2(H134R)-tdTomato-WPRE* or *ChR2-tdTomato* (stock #012567) were crossed to create the *Fgfr3-iCreER^{T2}; ChR2-tdTomato* mouse. Tamoxifen was injected intraperitoneally at 250 mg/kg on postnatal day 12 (P12) and P13 mice to visualize the expression of ChR2-tdTomato in cochleae at P28. Mice were genotyped as described in protocols by The Jackson Laboratory.

To induce ChR2-tdTomato expression specifically in mature DCs and PCs in the OoC, we used a previously characterized *Fgfr3-iCreER^{T2}* mouse line that displays ~100% inducible Cre activity in cochlear DCs and PCs when tamoxifen was injected at juvenile and adult ages (Cox et al., 2012; Walters et al., 2017). No ChR2-tdTomato was detected in DCs/PCs in *Fgfr3-iCreER^{T2}; ChR2-tdTomato⁺* control mice at P28, whereas *Fgfr3-iCreER^{T2+}; ChR2-tdTomato⁺* experimental mice showed robust expression of ChR2-tdTomato fusion protein specifically in both DCs and PCs within the OoC at P28 (see Fig. 1B–F).

The cochlear samples were fixed in 4% PFA for overnight at 4°C (P28 cochleae). Tissues were washed in PBS and decalcified in 120 mM EDTA, pH 7.4, for 48 h before microdissection of the OoC. The samples were blocked and permeabilized in the blocking buffer (10% FBS and 0.2% Triton X-100 in PBS) for 2 h at room temperature. They were then incubated at 4°C overnight with primary antibody Rabbit anti-Myosin VI (1:400 Proteus Bioscience). The tissues were incubated with 1:800 diluted secondary antibodies for 2 h at room temperature, washed with PBS, and incubated with DAPI (1:1000 Thermo Fisher Scientific) for 2 min at room temperature, washed with PBS, and then mounted for imaging using Fluoromount-G (Southern Biotechnology). All samples were imaged with an LSM700 confocal laser scanning image system (Carl Zeiss).

In vitro methods. Male and female mice aged at least P17 were killed using cervical dislocation. The mouse cochlea was freshly isolated and dissected in an ice-cold solution containing the following (in mM): 135 NaCl, 5.8 KCl, 1.3 CaCl₂, 0.9 MgCl₂, 0.7 NaH₂PO₄, 5.6 D-glucose, 10 HEPES, 2 sodium pyruvate, pH 7.5 (adjusted with NaOH) and osmolarity ~308 mOsm.

Our primary aim was to record DC electrical behavior under illumination within the syncytium. Accordingly, the dissected apical coil of the OoC was transferred to a microscope chamber, immobilized using a nylon mesh fixed to a stainless-steel ring and viewed using an upright microscope (Axioskope). Cells were observed with Nomarski differential interface contrast optics (40× water immersion objectives). The DCs are electrically coupled through connexin channels, and this coupling allows for the passage of molecules between the cells, as well as acting as an electrical syncytium (Santos-Sacchi, 1986). Indeed, Santos-Sacchi (1991) reported the increased potassium current amplitude when cells were coupled, attributing this to the junctional coupling between cells. The contribution of gap junctional coupling to the observed phenomena is beyond the scope of the present investigation, which is focused on the effects of ChR2 activation on the functioning of DCs. To mimic the *in situ* conditions, we recorded from a single DC in the intact isolated tissue, to assess the cellular effects of light activation of ChR2, which encodes a nonspecific cation conductance, on DCs electrical responses within the syncytium. Currents and membrane potentials were recorded using the same solution as for dissection. All recordings were made at room temperature (22°C). Patch pipettes were filled with an intracellular solution containing the following (in mM): 131 KCl, 3 MgCl₂, 5 Na₂ATP, 10 Na₂-phosphocreatine, 1 EGTA, 10 HEPES, 0.3 Na₂GTP, pH 7.3 (adjusted with KOH) and osmolarity ~293 mOsm. All chemicals were obtained from Sigma Aldrich. The patch pipettes were fabricated with a dual-stage glass micropipette puller (Narishige PC-100) using borosilicate glass with outer diameter 1.5 mm (Sutter Instruments) and heat polished with a microforge (Narishige MF-900). Currents were amplified with an Axopatch 700B amplifier (Molecular Devices) and filtered at a frequency of 2–5 kHz through a low-pass Bessel filter. The data were digitized at 5–500 kHz using an analog-to-digital converter (Digidata 1500; Molecular Devices). The whole-cell current recordings were conducted using pCLAMP software (version 10, Molecular Devices). No online leak-current subtraction was made, and only recordings with holding currents <50 pA at holding potentials of –90 mV were accepted for analyses.

This study included 18 cells with a series resistance (*R_s*) within a 5–15 MΩ range. After 60%–90% compensation of the mean residual, uncompensated *R_s* was 5.1 ± 0.5 MΩ. The seal resistance was typically 2–5 GΩ. The number of cells (*n*) is given for each dataset. Data were analyzed using pClamp10 (Molecular Devices), Origin9.1 (OriginLab), and Excel (Microsoft).

In voltage-clamp mode, cells were held at a membrane potential of –80 mV, and 10 mV step potentials were applied from –120 to 50 mV. For *in vitro* illumination of the preparation, we used a 470 nm, 50 mW laser source (Dragon Lasers) coupled to a fiber-optic cable (Thorlabs, M63L01, 105 μm, 0.22 NA), which was placed ~1.5 cm from the preparation. The fiber-tip location was adjusted with a micro positioner to illuminate the entire preparation. In both voltage and current clamp, cells were manually stimulated by shining the laser light for ~1 or 2 s. Laser power was adjusted between 0.2 and 1.7 mW mm^{–2} based on *in situ* calibration with a photodiode sensor power meter (Thorlabs, PM16-130). Since the light-induced currents showed a time-sensitive reduction in amplitude, we first determined the full functional recovery from this reduction. Using standard recovery protocol and testing different laser light density (0.25, 0.38, and 0.50 mW mm^{–2}), we observed that full recovery was almost achieved within 15 s (see Fig. 2D), and fully achieved in 30 s (not shown). The design of the stimulation protocol took this value into consideration, and thus was set to have 60 s between each voltage step. In current-clamp mode, cells were injected currents from –70 to 60 pA, in 10 pA increments.

In vivo physiologic recordings. Male and female mice at 3–5 weeks of age were anesthetized with ketamine (0.12 mg/g body weight, i.p.) and xylazine (0.01 mg/g body weight, i.p.) for nonsurgical procedures or with urethane (ethyl carbamate; 2 mg/g body weight, i.p.) for surgical procedures at the University of Brighton. Mice were tracheotomized, and their core temperature was maintained at 38°C. The auditory sensitivity of mice was assessed before surgery using distortion-product otoacoustic emissions (DPOAE, see below) to ensure each mouse was sensitive throughout the 1–70 kHz range of the sound system and especially

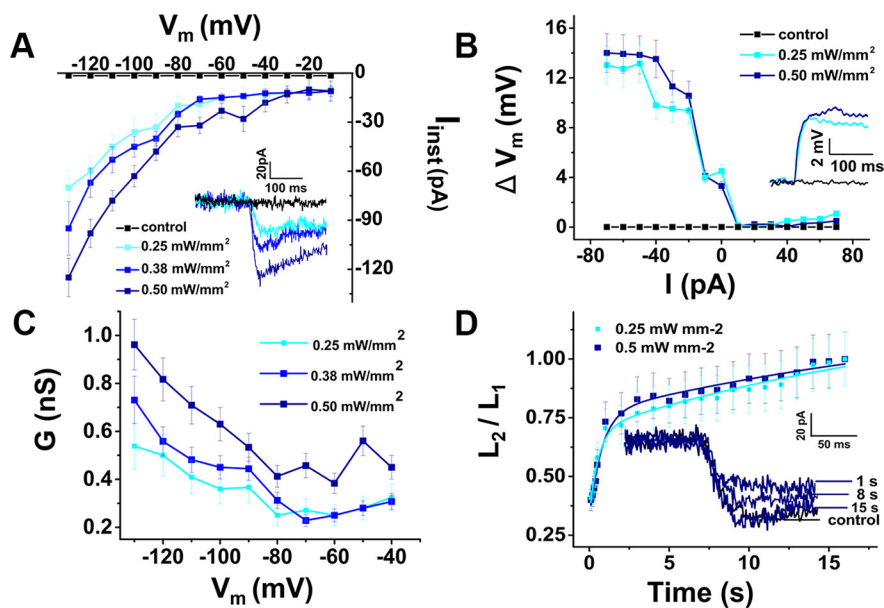


Figure 2. Light activation of ChR2 depolarizes ChR2 mouse DC membrane potentials *ex vivo*. **A**, Current-voltage (I - V) plot: peak current amplitudes (I_{inst}) of a DC in response to blue-light illumination at different power densities, as functions of the membrane potential (V_m). Average currents measured from a holding potential of -90 mV, at a step potential of -130 mV, for 0.25, 0.38, and 0.50 mW/mm² light intensity, were -70 ± 10 , -95 ± 16 , and -125 ± 12 pA, respectively, $n = 12$. Inset, Inward current traces at different blue-light power densities (-90 mV holding potential). **B**, Light-induced potential-current (ΔV_m - I) relationship of a DC: membrane-potential changes (ΔV_m) during blue-light illumination as functions of injected currents (I). Light-induced depolarizations were elicited during negative current injection. Average potential changes measured from resting membrane potential, at a current step of -80 pA 0.25 and 0.50 mW/mm² light intensity were 14.0 ± 1.6 and 13.0 ± 1.5 mV, respectively, $n = 6$. Inset, Whole-cell current-clamp recording (resting membrane potential of -50 mV) of light-elicited depolarization with different blue-light power densities. **C**, Conductance G as a function of membrane potential V_m at 3 different blue-light power densities using data in **A** at -90 mV holding potential. Increasing blue-light power increased the maximum measured DC membrane conductance at a step potential of -130 mV (0.54 ± 0.09 , 0.73 ± 0.09 , and 0.96 ± 0.11 nS, respectively, $n = 12$). **D**, ChR2 recovery kinetics after 1 s light stimulation in DCs at -90 mV holding potential using a standard recovery-time protocol. An initial 1 s light stimulation (L1) was followed by a second light stimulation (L2) after a time ranging from 0.1 to 17 s. The ratio of peak currents (I_2/I_1) elicited by L2 and L1 is plotted as a function of the interspike interval to show the recovery from L1. Inset, Examples of traces recorded in response to L2 after specified recovery times using 0.5 mW mm⁻² light intensity. The exponential fits to the data were τ_s for 0.25 mW mm⁻²: 0.54 ± 0.2 s, 23.05 ± 4.21 s ($n = 2$); for 0.50 mW mm⁻²: 0.78 ± 0.23 s, 27.43 ± 4.84 s ($n = 2$ cells).

sensitive to tones in the 50 kHz to 60 kHz range to levels ≤ 30 dB sound pressure level (SPL).

To measure BM displacements and the OoC cochlear microphonics, a caudal opening was made in the ventrolateral aspect of the right bulla to reveal the round window (Legan et al., 2000). Sound was delivered via a probe with its tip within 1 mm of the tympanic membrane and coupled to a closed acoustic system comprising two MicroTechGefell GmbH 1-inch MK102 microphones for delivering tones and a Bruel and Kjaer (www.Bksv.co.uk) 3135 0.25-inch microphone for monitoring sound pressure at the tympanum and DPOAEs. The sound system was calibrated *in situ* for frequencies between 1 and 70 kHz, and known sound-pressure levels were expressed in dB SPL with reference to 2×10^{-5} Pa. Tone pulses with rise/fall times of 1 ms were synthesized by a Data Translation 3010 (Data Translation) data acquisition board, attenuated, and used for sound-system calibration and the measurement of electrical and acoustical cochlear responses. To measure DPOAEs, primary tones were set to generate $2f_1 - f_2$ distortion products at frequencies between 1 and 50 kHz. DPOAEs were measured for f_1 levels from 10 to 80 dB SPL, with the levels of the f_2 tone set 10 dB below that of the f_1 tone. DPOAE threshold curves represented the level of the f_2 tone that produced a $2f_1 - f_2$ DPOAE with a level of 0 dB SPL when the f_2/f_1 frequency ratio was 1.23. System distortion during DPOAE measurements was 80 dB below the primary-tone levels.

The BM was illuminated by a blue 470 nm, 50 mW laser source (Dragon Lasers) couple to a fiber-optic cable (Thorlabs, M63L01, 105 μ m, 0.22 NA). The tip was positioned with a micromanipulator to be 0.2 mm from the surface of the RW membrane, where it cast a ~ 200 - μ m-diameter

circle of illumination on the BM, centered on either the micropipette or the BM displacement measurement beam. The distance of 0.2 mm from the RW was determined during the calibration of the beam by casting a 200 μ m diameter circle of illumination on the surface of the photo diode sensor of a power meter (Thorlabs, PM16-130). The laser power at the level of the OHCs was computed according to Wu et al. (2016), who used analysis and estimates provided by Zhang et al. (2007) and Aravanis et al. (2007). Laser on-off was controlled through transistor-transistor logic. If the illumination periods were extended for >3 s, the prolonged excitation of ChR2 and the gating of the nonselective cation conductances caused large, but reversible, changes in the electrochemistry of the cochlea (see Fig. 3B) that confounded the objective of using the technique for blocking ongoing DC and OPC function. For this reason, periods of BM light illumination were usually limited to ≤ 3 s.

Intracellular and extracellular voltage responses were recorded from presumed DCs and the fluid spaces of the OoC using glass pipettes (20–80 $\text{M}\Omega$ when filled with 3 M KCl) pulled from 1 mm diameter thin-walled quartz glass tubing on a Sutter P-2000 micropipette puller (Sutter Instrument). Signals were amplified with a recording bandwidth of DC – 100 kHz using a custom preamplifier (Brighton Lab, James Hartley). The voltage signals were not capacitance compensated. Presumed DCs with very negative resting membrane potentials (-112.5 ± 8.3 mV, $n = 18$) were encountered by advancing microelectrodes through the BM in the close vicinity of OHCs in the 50–60 kHz region of the basal turn of the cochlea. Further advance resulted in encountering the OoC fluid spaces that are adjacent to the OHCs, with zero potentials, and scala media with positive endocochlear potential (114.3 ± 3.7 mV, $n = 11$).

Tone-evoked BM displacements were measured by focusing the beam of a self-mixing, displacement sensitive, laser-diode interferometer (Lukashkin et al., 2005) through the round window membrane to form a 20 μ m spot on the center of the BM in the 50–60 kHz region of the cochlea. To take rapid snapshots of the BM responses without many averages, the following algorithm was used: The response amplitude of interferometer is largest when its operating point is situated in quadrature (Lukashkin et al., 2005). During recordings, the operating point fluctuated because of physiological noises in the preparation, and we constantly tracked for a response in, or very close to, quadrature (i.e., for the largest response). We balanced the demand for rapid data acquisition with the need for sensitive measurement by spotting the maximum response in 10–15 presentations of the same tone burst. The largest response amplitude recorded was the one closest to the quadrature response. This allowed us to complete recording of the entire level functions (dependence of the BM movement on stimulation level) within 15–20 s. The interferometer was calibrated at each measurement location by vibrating the piezo stack on which it was mounted over a known range of displacements. BM measurements were checked continuously for changes in the sensitivity of the measurement (because of changes in alignment or to fluid on the RW) and for changes in the condition of the preparation. If thresholds of the latter changed by >5 –10 dB SPL, the measurements were terminated. Tone pulses with rise/fall times of 1 ms were used for BM measurements. Stimulus delivery to the sound system and interferometer for calibration and processing of signals from the microphone amplifiers, microelectrode recording amplifiers,

and interferometer were controlled by a DT3010/32 (Data Translation) board by a PC running MATLAB (The MathWorks) at a sampling rate of 250 kHz. The output signal of the interferometer was processed using a digital phase-locking algorithm, and instantaneous amplitude and phase of the wave were recorded.

Measurements were made without knowledge of genotype. Less than 5% of all measurements were terminated because the physiological state of the preparation changed during measurements, in which case data from the sample was excluded.

Experimental design and statistical analyses

ChR2-tdTomato^{+/-} experimental mice were crossed to generate +/+, +/-, and -/- genotypes. Male and female mice were studied in approximately equal proportions. No phenotypic differences were observed between males and females. Physiologic tests were performed on +/- and -/- littermates to minimize any influence of age, environment, or genetic background. Tests were performed on 3- to 5-week-old mice to reduce the possibility of progressive loss of high-frequency responses, which is common in many mouse strains. Tests were performed on all mice in a litter without knowledge of genotype. The genotypes were determined after the experiments. For statistical analysis of physiological experiments, data were compared for at least 5 +/- and 5 ChR2^{-/-} mice, obtained from recordings of 2 or 3 complete litters. For analysis of BM and electrophysiological measurements from presumed DCs and fluid spaces of the OC, 18 +/- and 10 -/- ChR2 mice in total were tested. Data were analyzed as mean ± SD and plotted using Fig P (www.figpsoft.com) or Origin (www.originlab.com) software. Statistical tests were performed with GraphPad Prism (<https://www.graphpad.com/quickcalcs>) and comparisons made using unpaired *t* tests for unequal variances unless otherwise noted. *p* values are noted as absolute values with *t* values and degrees of freedom (df).

In summary, all measurements were performed blind. Measurements were made from each animal in a litter, and data were analyzed at the end of each set of measurements. When all measurements had been made from a particular litter, the tissue was genotyped. Phenotypic differences between the WT, heterozygous, and homozygous mice were very strong. Thus, only sufficient numbers of measurements were made to obtain statistically significant differences. Experiments were terminated (<5% of all measurements) if the auditory sensitivity of the preparation decreased by >10 dB SPL during a measurement and data from the measurement were excluded.

Software/code

For physiological recordings, data acquisition and data analysis were performed using a PC with programs written in MATLAB (The MathWorks). The programs are available on request from A.N.L. and I.J.R. The programs were written to communicate with specific hardware (Data Translation 3010 board and custom-made GPIB-controlled attenuators) and will need modification if used with different hardware.

Data and materials availability

All data are available in the main text. Additional data related to this paper may be requested from the authors.

Results

Specific inducible expression of ChR2 in cochlear supporting cells

To induce ChR2 expression specifically in mature DCs and PCs in the OoC of the cochlea, we used a previously characterized *Fgfr3-iCreER^{T2}* mouse line that displays ~100% inducible Cre

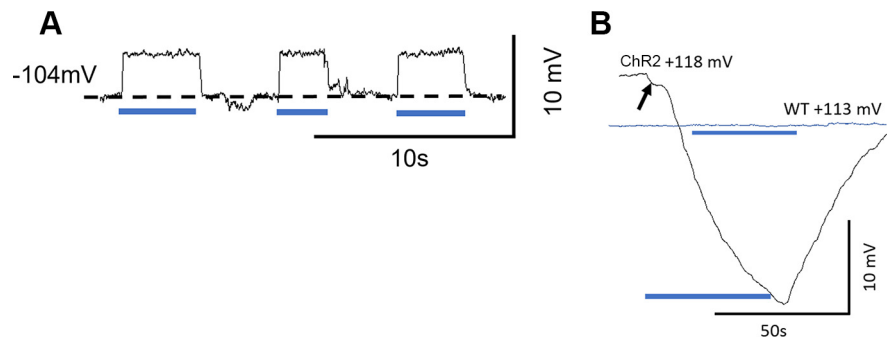


Figure 3. Light activation of ChR2 depolarizes ChR2 mouse DC membrane potentials *in vivo*. **A**, Examples of intracellular recordings from presumed DCs showing successive membrane depolarizations to OoC illumination. **B**, Prolonged OoC illumination and activation of ChR2 channels expressed in DCs and OPCs cause a large, slow reduction in the EP recorded from scala media during OoC illumination. ChR2 trace arrow indicates onset step. WT littermate (blue trace): nonresponsive to OoC illumination. **A, B**, Blue bars represent periods of illumination with a laser beam (200 μm diameter, 0.25 mW mm⁻², 470 nm).

activity in cochlear DCs and PCs when tamoxifen is injected at juvenile and adult ages (Cox et al., 2012; Walters et al., 2017). When induced at P12/P13 or P21, *Fgfr3-iCreER^{T2}*; *ChR2-tdTomato⁺* experimental mice showed robust expression of ChR2-tdTomato fusion protein specifically in both DCs and PCs within the OoC at P28, whereas no ChR2-tdTomato was detected in DCs/PCs in *Fgfr3-iCreER^{T2}*; *ChR2-tdTomato⁺* control mice at P28 (Fig. 1C–H; see Materials and Methods). No expression of ChR2-tdTomato was detected in stria vascularis or any other cochlear structures of *Fgfr3-iCreER^{T2}*; *ChR2-tdTomato⁺* experimental mice when induced at P12/P13 and analyzed at P21/P22. These results on ChR2-specific expression in DCs and PCs in the cochlea are consistent with previous studies (Hayashi et al., 2010; Cox et al., 2012; Walters et al., 2017).

ChR2 activation depolarizes ChR2 mouse DC membrane potentials in *ex vivo* and *in vivo* preparations

ChR2 is a light-sensitive, cation-selective channel (Nagel et al., 2002, 2003). When activated by light in whole-cell patch recordings from *ex vivo* flat-mounted preparations of the OoC, ChR2-expressing DCs are depolarized (Fig. 2A,B) by increased conductance (Fig. 2C). This was not observed in WT littermates (control, black traces, Fig. 2A,B).

In vivo measurements using sharp electrodes revealed that resting membrane potentials of mouse DCs (103.5 ± 7.3 mV, $n = 8$ DCs in 3 cochleae) were more negative than those recorded in the guinea-pig cochlea (Dallos et al., 1982). Depolarizations (Fig. 3A, 4.2 ± 0.3 mV, $n = 14$) were also recorded *in vivo* from presumed ChR2-expressing DCs when the ChR2 conductance was activated by OoC illumination. If the illumination periods were extended for >3 s, the prolonged excitation of ChR2 and the gating of the nonselective cation conductances caused large, but reversible, changes in the electrochemistry of the cochlea (Fig. 3B) that confounded the objective of using the technique for blocking ongoing DC and OPC activity. For this reason, periods of BM light illumination were usually limited to ≤ 3 s.

Activation of ChR2-expressing DCs and OPCs suppresses continuous fine adjustments of BM responses

To examine how supporting cells might influence cochlear mechanical responses, we measured the magnitude of BM displacement as a function of SPL. In contrast to RL frequency tuning (Ren et al., 2016), BM displacement frequency tuning curves closely mirror the voltage frequency tuning curves of OHCs

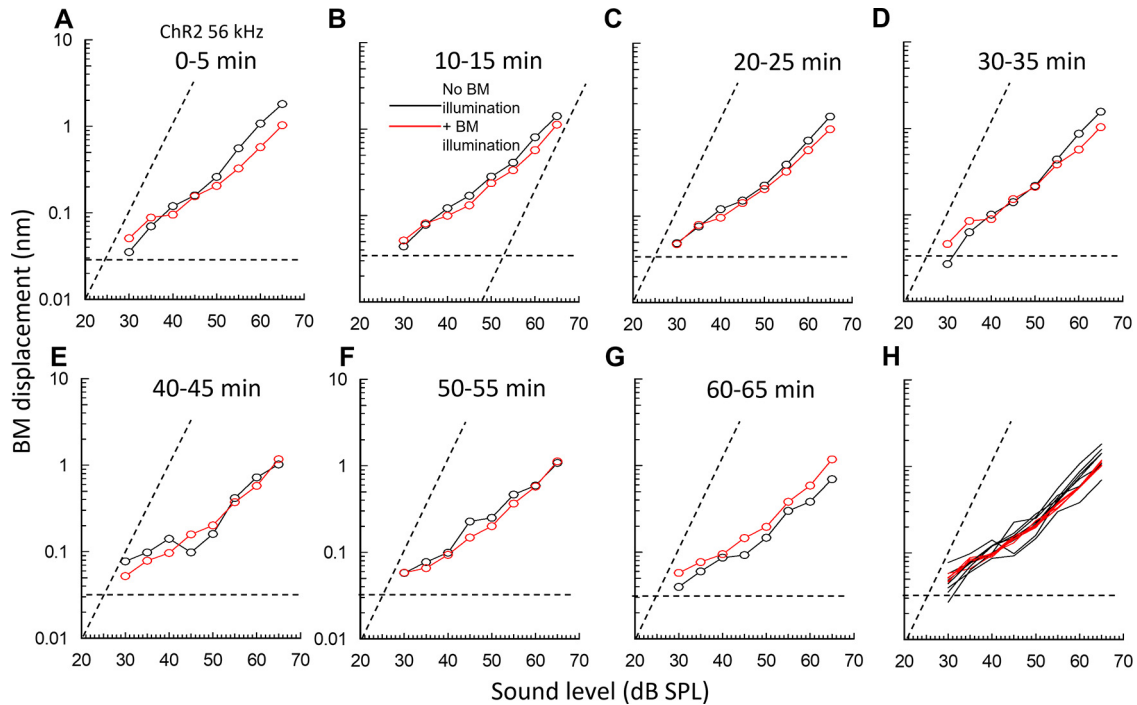


Figure 4. Light activation of Chr2 expressed in OPCs and DCs in Chr2 mice alters and stabilizes BM responses to tones. **A–G**, Successive BM displacement level functions to 56 kHz tones at 5 min intervals measured in a single preparation at the same 56 kHz BM location. Black symbols represent without OoC illumination. Red symbols represent with OoC illumination for >3 s. **H**, Traces **A–G**, superimposed. **A–G**, Dashed horizontal lines indicate averaged noise floors. Dashed transverse lines indicate slope of 1 dB/dB. OoC illumination: 200- μ m-diameter spot, 0.25 mW mm^{-2} , 470 nm wavelength.

(Russell and Kössl, 1992a; Russell et al., 1995). Thus, BM response to OoC illumination should reflect changes in OHC output because of light activation of Chr2 expressed in the supporting cells. A self-mixing laser vibrometer (Lukashkin et al., 2005) was used both in Chr2 mice that expressed Chr2 in their OPCs and DCs, and in their WT littermates that lacked such expression. We measured tone-evoked BM displacements both with and without activating the Chr2 conductance by OoC illumination (Fig. 4). To reduce the time interval between measurements, the number of iterative runs was reduced, which resulted in the raised noise floor.

Tone-evoked BM displacements in the basal turn of the cochlea were measured as a function of SPL to near-CF tones (Fig. 4), and a few kHz below CF (Fig. 5) before, during, and after BM illumination at the measurement site (Figs. 1A and 4). It was possible only to estimate the CF of the BM measurement location during the measurements. True CF was found offline during data analysis. In accordance with previous measurements from the mouse cochlea (e.g., Legan et al., 2000; Mellado Lagarde et al., 2014), BM level functions are compressive with slopes <1 for frequencies at and above CF (Fig. 4). For frequency just below CF and at levels >50 dB, when they are not subject to cochlear amplification, the slopes are close to 1 (Fig. 5).

Changes in BM mechanical responses occurred in Chr2 mice at OoC illumination onset, but responses returned close to the original control levels within 35 s of illumination offset. Measurements made from the cochleae of the same and different Chr2 mice revealed that, throughout the measured range (20–90 dB SPL), OoC illumination could both increase and decrease (Fig. 4A–G) BM mechanical responses to near-CF tones in the same cochlea by similar amounts (11.7 ± 4.1 dB, $n = 7$ cochleae for the increases and 13.2 ± 2.9 dB, $n = 9$ cochleae for the decreases). BM laser

illumination in WT littermates had no visible effects on the BM mechanical responses, which showed small variations in level functions regardless of the presence of the illumination (Fig. 5B). Any phase changes because of OoC illumination were ± 10 degrees and thus were within the noise floor of these measurements.

By measuring from the same cochlea successively over time at 5 min intervals (Fig. 4A–G), which enabled full recovery of BM mechanical responses following OoC illumination, and after superimposing the traces (Fig. 4H), we discovered that OoC illumination did not alter the overall sensitivity of the BM mechanical responses. Instead, it suppressed continuous fine control of BM mechanical responses over their entire measured range of sound levels. Without OoC illumination, successive level functions differed slightly. When successive illuminated BM level functions were superimposed (Figs. 4H and 5A,C, red curves and symbols), level functions obtained during OoC illumination were very similar, but not in WT littermates (Fig. 5B,D). When the mean and SDs of the superimposed level functions shown in Figure 5A, B were plotted (Fig. 5C,D), the mean curves lay almost over each other and the SDs overlapped. These findings indicate that there is no significant difference between the averaged BM responses to sound stimulation with and without OoC illumination for measurements made in Chr2 and WT mice. Importantly, however, the SDs of the averaged BM level functions measured during OoC illumination in Chr2 mice (Fig. 4C), but not in the WT mice (Fig. 5D), were significantly reduced compared with those measured without OoC illumination (see below).

To quantify the effect of Chr2 activation on fluctuations in BM mechanical responses (Figs. 4H and 5A,B), the SDs of measurements made at all levels throughout the level functions were expressed as a percentage of the mean (coefficient of variation

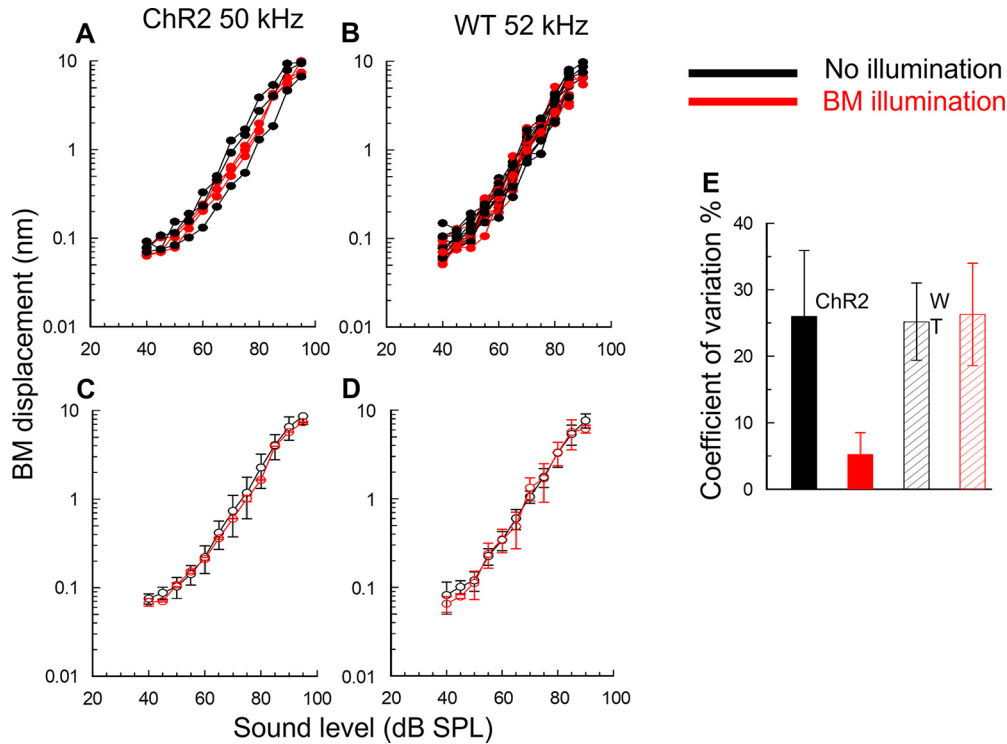


Figure 5. OoC illumination reduces the variability of basal turn BM responses in mice that express Chr2 in OPCs and DCs, but not in WT littermates. **A, B.** Superimposed successive level functions (BM displacement as a function of tone SPL), measured from the basal BM turns (at 5 min intervals) in a Chr2 mouse (**A**) and a WT littermate (**B**), without (black curves) and with (red curves) OoC illumination. All measurements were made at frequencies below the CF of the measurement location (55–57 kHz). Dashed transverse lines indicate slope of 1 dB/dB. **C, D.** Mean \pm SD of curves presented in **A, B**. **E.** CV. Chr2: without OoC illumination (black solid); with OoC illumination (red solid). WT: without OoC illumination (black hatched); with OoC illumination (red hatched). OoC illumination: 200- μ m-diameter spot, 0.25 mW mm $^{-2}$, 470 nm wavelength.

[CV]). Based on five BM displacement-level functions measured during, five before, and five after OoC illumination, in each of 5 Chr2 mice (a total of 75 level functions), the CV calculated for the entire range of level functions was $26.0 \pm 9.9\%$ ($n = 50$) without OoC illumination and $5.2 \pm 3.9\%$ ($n = 25$) with OoC illumination (Fig. 5E). The CV during OoC illumination (i.e., Chr2 activation) is significantly smaller than that without illumination (two-tailed t test, $p > 0.0001$, $t = 9.4702$, $df = 73$). Similar analysis of 5 WT littermates revealed no significant difference in the CV in BM displacement measurements made without ($25.2 \pm 5.8\%$, $n = 50$) and with OoC illumination ($26.3 \pm 7.7\%$, $n = 25$) (two-tailed t test, $p = 0.4909$, $t = 0.6923$, $df = 73$). Accordingly, light activation of Chr2 expressed in DCs and OPCs suppresses DC- and OPC-mediated fine adjustments in BM mechanical responses and stabilizes BM displacement-level functions.

Light activation of Chr2-expressing DCs and OPCs suppresses continuous adjustments to actively amplified OHC electrical responses

OHCs are mechanically caged by the DCs and OPCs and are suggested to exchange forces via this cage with the TM and BM of the cochlear partition (Soons et al., 2015; Motallebzadeh et al., 2018; Wang et al., 2021). For this reason, as a first step in understanding how DCs and OPCs might control OHC sensitivity *in vivo*, we measured the effects of activating the Chr2 receptors expressed in the DCs and OPCs, on OHC tone-evoked voltage responses. The measured voltage response corresponds to the ERP, which is produced across the resistive network of the CL (see Introduction). We measured the magnitude of ERPs recorded from the CL of Chr2 mice and their WT littermates

using thin-walled quartz micropipettes (resistances: 30–60 M Ω , 3M KCl electrolyte). The ERP was expressed as a function of SPL (level functions) in response to tones with and without Chr2 activation in the 50–60 kHz region of the cochlea. The largest tone-evoked voltage ERPs recorded from the OoC were from the CL immediately adjacent to the OHCs and DCs (Johnstone et al., 1989). Because of the spread of excitation, with increasing level $> \sim 40$ dB SPL, OHCs from adjacent frequency regions contributed to the ERP (Cheatham et al., 2011). In 9 sensitive mice (thresholds at the CF of the measurement location = 16.5 ± 3.2 dB SPL), continuous light activation of Chr2 expressed in the DCs and OPCs caused changes in the ERP responses to 50–60 kHz tones for stimulus levels within ~ 30 dB SPL of threshold (Fig. 6A). Similar to the stabilization effect of Chr2 light activation on the BM level functions in the Chr2 mice (Figs. 4H, 5), Chr2 light activation stabilized OHC voltage responses to tones. They differed, however, by stabilizing ERPs only to tones at and close to the CF that are subject to amplification (Fig. 6A). OoC illumination had no apparent effect on ERPs outside this range or to ERPs recorded in response to tones at any frequency or level from WT littermates (Fig. 6B). The stabilization revealed that OPCs and DCs can adjust the threshold ERP response through decreasing it by a maximum of 14.1 ± 3.3 dB ($n = 7$ cochleae) or increasing it by a maximum of 12.4 ± 3.2 dB ($n = 8$ cochleae). Within 35 s of OoC illumination, ERP sensitivity returned to levels similar to those before OoC illumination demonstrating its reversibility.

To quantify the effect of Chr2 activation on ERP level-function fluctuation, we measured the mean \pm SD at each measurement level of the successive groups of level functions (Fig. 6C,D). From inspection of Figure 6C for levels within 30 dB of the detection threshold, the SDs of measurements made with Chr2

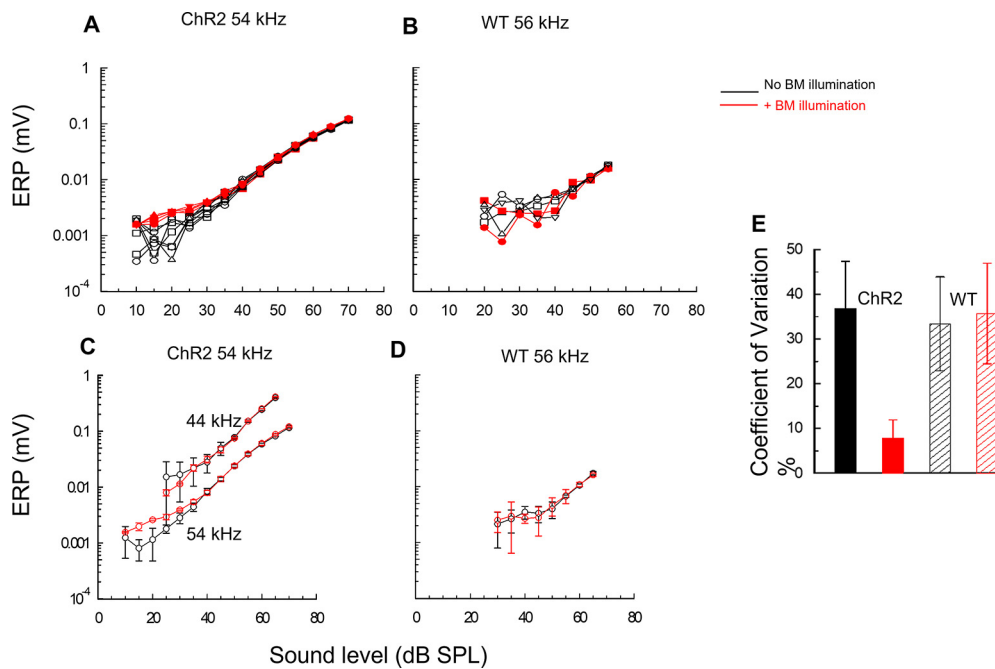


Figure 6. Light activation of ChR2-expressing DCs and OPCs suppresses continuous adjustments to actively amplified OHC electrical responses. **A, B**, superimposed succession of alternating measurements of ERP magnitude to tonal stimulation at 54 kHz from the 54 kHz BM location of a ChR2 mouse as a function of SPL, spaced at 5 min intervals, without and with OoC illumination (**A**), and for tonal stimulation at 56 kHz from the 56 kHz BM location of a WT littermate (**B**). **C, D**, Mean \pm SD of data shown in **A, B**, with the addition of (**A**) mean \pm SD for responses to 44 kHz at the 54 kHz location. **E**, CV. ChR2: without OoC illumination (black solid); with OoC illumination (red solid). WT: without OoC illumination (black hatched); with OoC illumination (red hatched). All measurements were uncompensated for and electrode characteristics. **C, D**, $n = 6$ without OoC illumination and $n = 5$ with OoC illumination. OoC illumination: 200 μ m beam diameter, wavelength: 473 nm, power density = 0.25 mW mm⁻².

activation were considerably smaller than those made without. For ERP measurements to levels above this range, the SDs of ERP measurements made with and without ChR2 activation were similar. The relative SDs of measurements within 30 dB of the measurement threshold were expressed as CVs (Fig. 6E). Based on ERP level functions measured before, during, and after ChR2 activation, in each of 5 ChR2 mice (a total of 42 level functions), the CV was $36.9 \pm 15.0\%$ ($n = 28$) for ERP level functions in the 30 dB range of the ERP detection threshold without ChR2 activation, and $7.9 \pm 4.0\%$ ($n = 14$) for those with ChR2 activation. The CV during ChR2 activation was significantly smaller than that without ChR2 activation (two-tailed t test, $p > 0.0001$, $t = 6.9716$, $df = 40$). Similar analysis of 5 WT littermates that do not express ChR2 revealed no significant difference in the CV (Fig. 6E) in ERP level functions made without OoC illumination ($33.4 \pm 10.5\%$, $n = 32$) and with OoC illumination ($35.7 \pm 11.3\%$, $n = 16$) (two-tailed t test, $p = 0.5053$, $t = 0.6714$, $df = 46$). It is concluded that light activation of ChR2 expressed in DCs and OPCs blocks fluctuations in the ERP displacement-level functions at levels that are subject to active amplification. Accordingly, DCs and OPCs fine-control cochlear amplification at near-threshold levels.

Light activation of ChR2 reveals a role for DCs and OPCs in recovery from temporary noise-induced cochlear desensitization

It has been suggested that OoC supporting cells play a role in the recovery of cochlear sensitivity from temporary acoustic desensitization (Flock et al., 1999). Motivated by the findings reported above, we tested the idea that OPCs and DCs contribute to recovery from temporary acoustic desensitization through homeostatic control of the electrochemistry of the CL. To this end, we examined the consequences for recovery

from temporary cochlear desensitization in ChR2 mice by activating the ChR2 conductance expressed in OPCs and DCs to effectively interfere with their normal function during the recovery period. Brief exposure to loud sounds (≥ 80 dB SPL) can temporarily desensitize the cochlea for seconds to minutes (Cody and Russell, 1988). Cochlear desensitization of ~ 15 dB (Fig. 7A–C, green arrows) and associated timelines measured at 70 dB SPL (Fig. 7D–F) occurred when the required 5 min recovery period between successive level function measurements (which included exposure to ≥ 80 dB SPL sounds) was omitted. In Figure 7B, it is shown that the cochlear BM responses are desensitized if a second level function is measured (open circles) within 35 s of the initial measurement (open squares), as observed in Figure 7A. Measurement of a level function (open red squares, 105 s) immediately following ChR2 activation by a brief period (3 s) of OoC illumination revealed that ChR2 activation in the OoC supporting cells was associated with rapid recovery from the temporary desensitization (open black circles, 70 s). The OoC illumination period is shown as a vertical red bar in the associated timeline (Fig. 7E). All preparations, either through slow or rapid recovery, recovered to control levels by 5 min (solid black squares). Rapid recovery from loud-sound desensitization did not occur if OoC illumination of a ChR2 mouse was omitted (Fig. 7A, D). WT littermates that did not express ChR2 in OoC supporting cells also failed to recover rapidly if the OoC was illuminated (Fig. 7C, open red squares; and Fig. 7F, vertical red bar in associated timeline). Bar charts shown in Fig. 7G represent the maximum decrease (\pm SD) in BM displacement sensitivity to near-CF tones following presentation of three successive level function measurements at 35 s intervals in ChR2 mice (15.3 ± 3.4 dB, $n = 6$ cochleae) and WT littermates (14.9 ± 3.7 dB, $n = 5$) without OoC illumination, and in ChR2

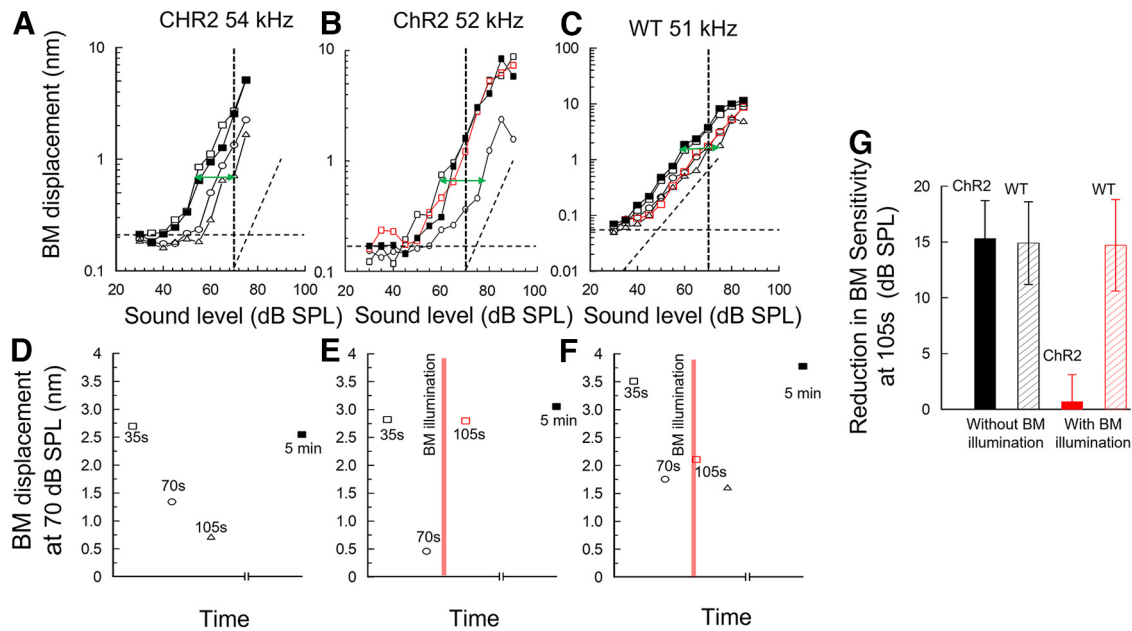


Figure 7. Light activation of Chr2-expressing supporting cells accelerates recovery of cochlea temporarily desensitized by loud sound. **A, B,** Succession of BM displacement level functions measured in the cochlea of a Chr2 mouse without OoC illumination (**A**) and with OoC illumination (**B**). **C,** WT littermate with OoC illumination. Dashed transverse lines indicate slope of 1 dB/dB. **A, B,** Black open squares represent first (35 s) level function measurement. Black open circles represent second (70 s) measurement. Black open triangles represent third (105 s) measurement. Solid black squares represent level function measured 5 min later. See accompanying timelines (**D–F**, below **A–C**) of BM displacement (nm) measured at 70 dB SPL (**A–C**, vertical dashed lines) as a function of the time. **E, F,** Red vertical bars represent 3 s period of OoC illumination. **A–C,** Green arrows indicate maximum change in sensitivity. Horizontal dashed lines indicate recording noise floor. Vertical axes are optimized for scale. **G,** Bar graphs represent maximum decrease in BM displacement sensitivity to near-CF tone level functions measured at 105 s, after three level function measurements, in Chr2 mice (solid black) and WT littermates (hatched black) without OoC illumination and in Chr2 (solid red) and WT (hatched red) mice with OoC illumination. OoC illumination: 200 mm beam diameter, wavelength: 473 nm, power density = 0.25 mW mm⁻².

(0.7 ± 2.4 dB, $n = 6$) and WT littermates (14.7 ± 4.1 dB, $n = 5$) with OoC illumination preceding the third level function measurement. There was no significant difference in the sensitivity decrease following loud-tone exposure between the WT and Chr2 mice without OoC illumination (two-tailed t test, $p = 0.7964$, $t = 0.2658$, $df = 9$). The sensitivity decreases following loud-tone exposure with OoC illumination in Chr2 mice and in WT littermates was very significantly different (two-tailed t test, $p < 0.0001$, $t = 8.5932$, $df = 10$). DCs and OCs are thus involved in producing the period of desensitization in the prolonged recovery period that follows exposure of the cochlea to a loud sound.

Light activation of Chr2-expressing DCs and OPCs changes the polarity of tonic electrical potentials, but not ERPs, recorded in the CL

When tone levels increase from moderate to intense, the almost symmetrical ERPs recorded adjacent to OHCs in the basal turn of the cochlea become positively asymmetrical and generate an extracellular tonic receptor potential (ERPDC) that appears instantaneously positive at tone onset and declines with time (Russell et al., 1986; Russell and Kössl, 1992b), as observed also in the mouse cochlea (Fig. 8A–E). Thus, immediately from tone onset, the net current outflow across the basolateral membranes into the CL exceeds net current inflow. The mechanism responsible for this change in symmetry has been attributed to a level-dependent change in the operating point of the OHC MET conductance, possibly caused by a tonic radial shear displacement between the RL and TM that causes tonic hair bundle displacement in the inhibitory direction (Cody and Russell, 1987; Russell and Kössl, 1992b). Following the sudden positive potential at tone onset, the magnitude of the ERPDC declines over time. At tone offset, the ERPDC

became suddenly negative, presumably because the net radial shear between the RL and TM, and consequently the OHC MET conductance operating point, returns to their resting states, and declines over a time scale similar to that observed during the tone burst (Fig. 8A–E). The time-dependent declines in net current outflow during the tone burst and net current inflow across the OHC basolateral membranes from the CL at tone offset has been attributed to the accumulation of K⁺ in, and its removal from, the CL (Cody and Russell, 1988; Johnstone et al., 1989). When Chr2 expressed in the DCs and OPCs is activated, the sign of the ERPDC is reversed and becomes sharply negative on tone onset and positive at offset and declines in magnitude over time (Fig. 8D,E), as observed for the ERPDC without Chr2 activation. It is possible that light activation of Chr2 expressed in DCs and OPCs alters the mechanical properties of the OoC, as discussed below, which causes a net radial shear between the RL and TM such that the OHC hair bundles, and hence the OHC MET operating point, are instantaneously biased in the excitatory direction. For frequencies at and close to the CF of the recording site, and for low-to-moderate level tones, OoC illumination influences the magnitude of the phasic ERP without altering the magnitude and sign of the ERPDC. However, at these same frequencies, and for moderate to intense tones, OoC illumination changes the polarity of the ERPDC with little or no apparent influence on the magnitude and phase of ERPs (Fig. 8F,G).

Discussion

Optogenetics reveal DCs and OPCs finely and continuously control cochlear sensitivity

To our knowledge, our report here is the first successful application of optogenetics to studying OoC function *in vivo*. By gating the large Chr2 cationic channels expressed in the DCs and OPCs of Chr2 mice, we revealed the normal function of DCs

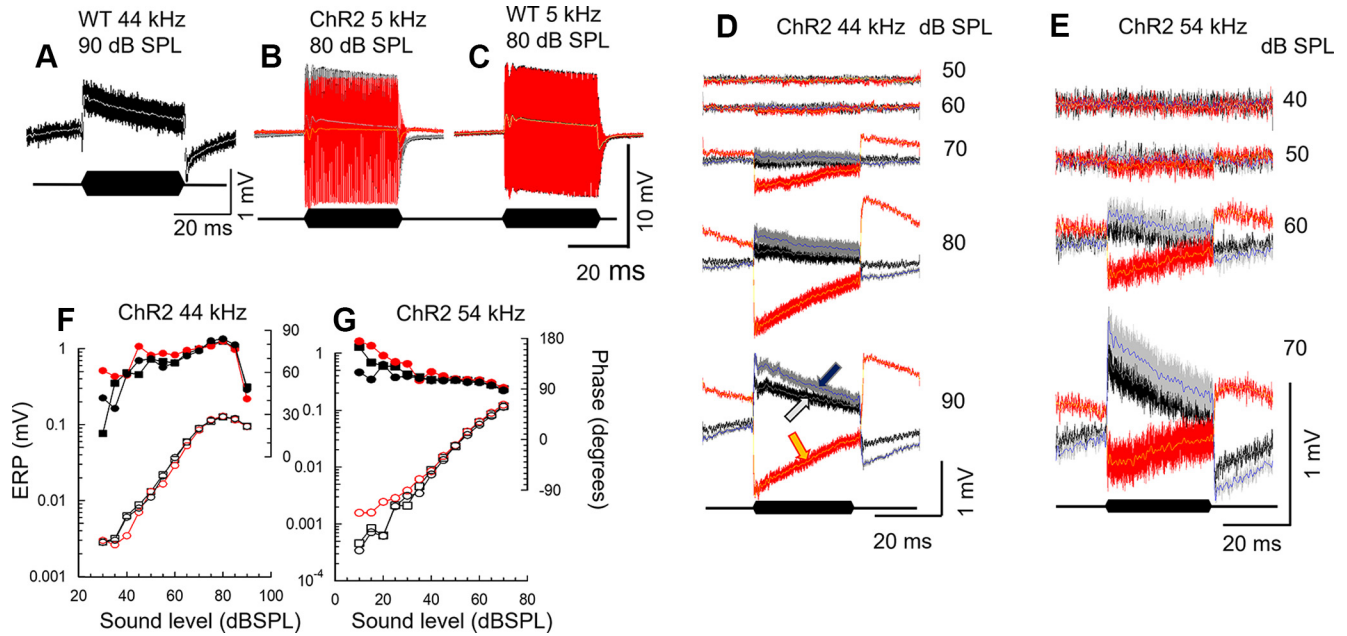


Figure 8. Light activation of Chr2-expressing DCs and OPCs changes the polarity of tonic electrical potentials recorded in the CL. **A–E**, ERP recorded from the CL in WT littermates (**A,C**) and Chr2 mice (**B,D,E**) to tones at frequencies and levels indicated. ERP before (black), during (red), and after (gray) OoC illumination. Traces are superimposed with 1 kHz, low-pass (LP) filtered ERPDC before (white), during (yellow), and after (blue) OoC illumination, indicated by white, yellow, and blue arrows, respectively, in **D** (90 dB SPL). Black lozenges represent tone bursts. **D, E**, Sequences of ERP to tones of increasing levels before, during, and after OoC illumination. **F, G**, ERP magnitude and phase measured from **D** and **E**, respectively, as functions of SPL. Phase is measured with respect to sound stimulus command voltage. BM blue light illumination: 200 μm beam diameter, wavelength: 473 nm, power density: 0.25 mW mm^{-2} . Measurements were not corrected for middle-ear and electrode characteristics.

and OPCs concerns continuous, fine regulation of BM mechanical and OHC voltage responses (Figs. 4–6). DCs and OPCs are involved in finely regulating cochlear partition mechanical responses over their entire dynamic range but control OHC voltage responses only over the low-to-moderate sound levels that are subject to amplification. At moderate-to-high sound levels, DCs and OPCs control OHC voltage response symmetry by controlling the radial shear between the TM and RL. These findings indicate that at low sound levels, DCs and OPCs control cochlear amplification, but, at higher sound levels, DCs and OPCs can induce mechanical changes in the cochlear partition that influence only the operating point of the OHC MET.

Fine regulation of the OHC voltage and BM mechanical responses

DCs exhibit Ca^{2+} -dependent deformation (Dulon et al., 1994). Depolarization causes mechanical changes in isolated DCs that include increases in the curvature of the DC phalangeal processes (Dulon et al., 1994; Bobbin, 2001; Yu and Zhao, 2009). From *in vitro* studies of isolated DC/OHC pairs, mechanical stimulation and/or depolarization cause mechanical changes in DCs that modulate OHC turgor pressure (Yu and Zhao, 2009), which controls OHC electromotility and, hence, cochlear amplification (Kakehata and Santos-Sacchi, 1995). It is proposed that such interaction between DCs and OHCs could account for the fine adjustment in the sensitivity we have observed in OHC voltage responses and associated BM mechanical responses (Figs. 4–6).

DCs regulate BM mechanical, OHC voltage responses, and ERP symmetry

From the studies on isolated cells and preparations mentioned above, DC deformation *in vivo* could be controlled by changes in the electrochemistry of the CL, notably the electrical polarization, and K^+ levels of the CL, which change in response to

acoustic stimulation (Cody and Russell, 1988; Johnstone et al., 1989). OHCs generate a tonic component (ERPDC) of the ERP in response to acoustic stimulation by moderate to high level sounds. The ERPDC is associated with depolarization and increased K^+ levels in the CL (Cody and Russell, 1985, 1988, 1995; Johnstone et al., 1989). The sharp rise and fall of the ERPDC at tone onset and offset and its decline during and following the tone, as reported here (Fig. 8) and in earlier studies, can be explained as follows. Depolarization of the CL is because of K^+ accumulation (Johnstone et al., 1989), presumably when the inward flow of K^+ , due primarily to the gating of the OHC MET channels, exceeds outflow because of K^+ clearance by electro-neutral K^+/Cl^- cotransporters in the adjacent DCs (Boettger et al., 2002, 2003). K^+ clearance is presumed to be facilitated by constant K^+ clearance from the DC cytoplasm via an intercellular gap-junctional pathway (Jagger and Forge, 2006). The ERPDC arises because the ERP changes from being almost symmetrical to positively asymmetrical. The mechanism responsible for this symmetry change was attributed to a level-dependent inhibitory shift of the OHC MET conductance operating point caused by tonic radial shear displacement between the RL and TM (Cody and Russell, 1988; Russell and Kössl, 1992b) because of voltage-dependent OHC shortening (Santos-Sacchi and Dilger, 1988). This conclusion was supported by the discovery that the ERPDC was mirrored exactly in the responses of the receptor potentials of adjacent inner hair cells (IHCs), which became more symmetrical (Cody and Russell, 1995). Increased symmetry caused a decline in the DC component of the IHC receptor potential, resulting in decreased sensitivity of the auditory system to moderate to high level sounds. A role for interaction between DCs and OHCs is strongly implicated in the control of the symmetry of OHC and IHC receptor potentials because activation of

Chr2 expressed in DCs and OPCs controls the OHC MET operating point, which reverses the polarity of the ERPDC from normally positive to negative.

How DCs contribute to the shear displacement between the TM and RL at high levels is unknown. DCs could exert forces on OHCs to increase turgor pressure and modify their electromotility. In addition, modeling studies have indicated that DC mediated forces acting through their phalangeal processes against the RL could alter the gain of cochlear amplification perhaps locally or through longitudinal coupling (Motallebzadeh et al., 2018). The reversal in polarity of the ERPDC can be accounted for by the gating of the large Chr2 cationic conductance expressed in the DCs, which would effectively shunt K^+ from the CL and increase the driving voltage for K^+ across the OHC basolateral membrane and hyperpolarize the OHCs. OHCs elongate when hyperpolarized (Santos-Sacchi and Dilger, 1988), which could reverse radial shear between the TM and RL and shift the OHC MET conductance operating point in the inhibitory direction. If, as we anticipate, fine control of cochlear sensitivity depends on K^+ levels in the CL, this may explain why cation channels are not expressed in DCs and OPCs in high densities (Nenov et al., 1998), because these could short-circuit the mechanism that fine-controls cochlear sensitivity. Another reason for the limited K^+ buffering abilities of supporting cells might originate from an apparent lack of selective evolutionary pressure to favor the expression of a system that ensures rapid recovery from temporary threshold shift (see below). This is because acoustic stimulation loud enough to cause a temporary threshold shift is normally absent in animal natural habitats. An intriguing hypothesis requiring investigation is that OHCs and DCs together form a control system that is mediated by CL K^+ levels. We propose increased levels of OHC excitation increase CL K^+ levels, thereby stimulating K^+ clearance from the CL and corresponding adjustments in OHC power output. Voltage and K^+ measurements from the CL (Cody and Russell, 1988; Johnstone et al., 1989) reveal the rate of K^+ influx because of OHC MET activation always exceeds that of K^+ clearance. We further conjecture, because of OHC MET activation, CL K^+ levels directly and/or indirectly control electromechanical feedback between the DCs and OHCs. This control appears as minor corrections to BM displacements throughout the dynamic range of BM responses to sound and as fine-tuning of OHC voltage responses to tones at levels subject to cochlear amplification.

DCs and OPCs and impedance matching between the OHCs and their supporting-cell scaffold

In parallel with changes in OHC electromechanical sensitivity (Yu and Zhao, 2009), changes in the mechanical properties of the DCs and OPCs have been proposed to alter impedance matching between the OHCs and their supporting-cell scaffold (Ramamoorthy and Nuttall, 2012). Similar effects *in vivo* could account for our findings that: (1) OHC voltage responses to CF and near-CF tones are sensitive to Chr2 light activation only over levels within 30–40 dB SPL of their thresholds; and (2) BM displacements are sensitive to light activation over their entire dynamic range and at levels and frequencies that have no observable influence on the magnitude and phase of OHC ERP. These findings indicate that DCs and OPCs can induce mechanical changes in the cochlear partition that influence only the operating point of the OHC MET.

Organ of Corti supporting cells mediate recovery from temporary desensitization

The high-frequency region of the mouse cochlea is especially susceptible to temporary desensitization, which was also observed in guinea pigs (Cody and Russell, 1985, 1988, 1995). For this reason, 5 min were interposed between each level-function measurement; otherwise, the cochlea became desensitized. OoC illumination in Chr2 mice, but not WT littermates, restored sensitivity almost immediately after a level-function measurement without a rest interval (Fig. 7). Perhaps Chr2 activation causes rapid K^+ removal from the CL, as proposed above, and it is sound-induced K^+ elevation in the CL that initiates and controls OPCs and DCs in the recovery from cochlear temporary desensitization.

This finding indicates roles for DCs and OPCs in the desensitization process that may be important for the long-term preservation of cochlear sensitivity and hearing, consistent with reported effects when DCs/OPCs are destroyed experimentally (Mellado Lagarde et al., 2014). Moreover, the interaction between supporting cells and OHCs has been studied at molecular levels. Breglio et al. (2020) demonstrated that exosomes are released from supporting cells that contain signaling molecules for protection against trauma or cisplatin insults. Further studies are clearly required to fully elucidate the mechanisms by which OoC supporting cells control the mechanical, electrical, and ionic environment of the OHCs, and the external factors that initiate this control. These studies are essential to better understand the normal function of OoC supporting cells in cochlear sensory processing. Their role should not be ignored in attempts to restore hearing function by repairing and regenerating sensory hair cells. Optogenetics could offer new opportunities in both the investigation of normal and abnormal function in the cochlea and its eventual treatment.

References

- Aravanis AM, Wang LP, Zhang F, Meltzer LA, Mogri MZ, Schneider MB, Deisseroth K (2007) An optical neural interface: in vivo control of rodent motor cortex with integrated fiberoptic and optogenetic technology. *J Neural Eng* 4:S143–S156.
- Ashmore J (2008) Cochlear outer hair cell motility. *Physiol Rev* 88:173–210.
- Beurg M, Fettiplace R, Nam JH, Ricci AJ (2009) Localization of inner hair cell mechanotransducer channels using high-speed calcium imaging. *Nat Neurosci* 12:553–558.
- Bobbitt RP (2001) ATP-induced movement of the stalks of isolated cochlear Deiters' cells. *Neuroreport* 12:2923–2926.
- Boettger T, Hübner CA, Maier H, Rust MB, Beck FX, Jentsch TJ (2002) Deafness and renal tubular acidosis in mice lacking the K-Cl co-transporter Kcc4. *Nature* 416:874–878.
- Boettger T, Rust MB, Maier H, Seidenbecher T, Schweizer M, Keating DJ, Faulhaber J, Ehmke H, Pfeiffer C, Scheel O, Lemcke B, Horst J, Leuwer R, Pape HC, Völkl H, Hübner CA, Jentsch TJ (2003) Loss of K-Cl co-transporter KCC3 causes deafness, neurodegeneration and reduced seizure threshold. *EMBO J* 22:5422–5434.
- Breglio AM, May LA, Barzik M, Welsh NC, Francis SP, Costain TQ, Wang L, Anderson DE, Petralia RS, Wang YX, Friedman TB, Wood MJ, Cunningham LL (2020) Exosomes mediate sensory hair cell protection in the inner ear. *J Clin Invest* 130:2657–2672.
- Cheatham M, Naik K, Dallos P (2011) Using the cochlear microphonic as a tool to evaluate cochlear function in mouse models of hearing. *J Assoc Res Otolaryngol* 12:113–125.
- Cody AR, Russell IJ (1985) Outer hair cells in the mammalian cochlea and noise-induced hearing loss. *Nature* 315:662–665.
- Cody AR, Russell IJ (1987) The response of hair cells in the basal turn of the guinea-pig cochlea to tones. *J Physiol* 383:551–569.

- Cody AR, Russell IJ (1988) Acoustically induced hearing loss: intracellular studies in the guinea pig cochlea. *Hear Res* 35:59–70.
- Cody AR, Russell IJ (1995) Time-varying voltage responses of mammalian hair cells to isoamplitude acoustic stimulation. *Aud Neurosci* 1:351–361.
- Corey DP, Hudspeth AJ (1979) Ionic basis of the receptor potential in a vertebrate hair cell. *Nature* 281:675–677.
- Cox BC, Liu Z, Mellado Lagarde MM, Zuo J (2012) Conditional gene expression in the mouse inner ear using Cre-loxP. *J Assoc Res Otolaryngol* 13:295–322.
- Dallos P (2008) Cochlear amplification, outer hair cells and prestin. *Curr Opin Neurobiol* 18:370–376.
- Dallos P, Santos-Sacchi J, Flock Å (1982) Intracellular recordings from cochlear outer hair cells. *Science* 218:582–584.
- Davis HA (1965) Model for transducer action in the cochlea. *Cold Spring Harb Symp Quant Biol* 30:181–190.
- Dulon D, Blanchet C, Laffon E (1994) Photoreleased intracellular Ca^{2+} evokes reversible mechanical responses in supporting cells of the guinea-pig organ of Corti. *Biochem Biophys Res Commun* 201:1263–1269.
- Eckhard A, Gleiser C, Rask-Andersen H, Arnold H, Liu W, Mack A, Müller M, Löwenheim H, Hirt B (2012) Co-localisation of K(ir)4.1 and AQP4 in rat and human cochlea reveals a gap in water channel expression at the transduction sites of endocochlear K^{+} recycling routes. *Cell Tissue Res* 350:27–43.
- Flock Å, Flock B, Fridberger A, Scarfone E, Ulfendahl M (1999) Supporting cells contribute to control of hearing sensitivity. *J Neurosci* 19:4498–4507.
- Hayashi T, Ray CA, Younkins C, Bermingham-McDonogh O (2010) Expression patterns of FGF receptors in the developing mammalian cochlea. *Dev Dyn* 239:1019–1026.
- Hibino H, Kurachi Y (2006) Molecular and physiological bases of the K^{+} circulation in the mammalian inner ear. *Physiology (Bethesda)* 21:336–345.
- Jagger DJ, Forge A (2006) Compartmentalized and signal-selective gap junctional coupling in the hearing cochlea. *J Neurosci* 26:1260–1268.
- Johnstone BM, Patuzzi R, Syka J, Syková E (1989) Stimulus-related potassium changes in the organ of Corti of guinea-pig. *J Physiol* 408:77–92.
- Kakehata S, Santos-Sacchi J (1995) Membrane tension directly shifts voltage dependence of outer hair cell motility and associated gating charge. *Biophys J* 68:2190–2197.
- Legan PK, Lukashkina VA, Goodyear RJ, Kössl M, Russell IJ, Richardson GP (2000) A targeted deletion in [alpha]-tectorin reveals that the tectorial membrane is required for the gain and timing of cochlear feedback. *Neuron* 28:273–285.
- Lukashkin AN, Bashtanov ME, Russell IJ (2005) A self-mixing laser-diode interferometer for measuring basilar membrane vibrations without opening the cochlea. *J Neurosci Methods* 148:122–129.
- Mellado Lagarde MM, Wan G, Zhang LL, Gigliello AR, McInnis JJ, Zhang Y, Bergles D, Zuo J, Corfas G (2014) Spontaneous regeneration of cochlear supporting cells after neonatal ablation ensures hearing in the adult mouse. *Proc Natl Acad Sci USA* 111:16919–16924.
- Mistrik P, Ashmore JF (2009) The role of potassium recirculation in cochlear amplification. *Curr Opin Otolaryngol Head Neck Surg* 17:394–399.
- Motallebzadeh H, Soons JA, Puria S (2018) Cochlear amplification and tuning depend on the cellular arrangement within the organ of Corti. *Proc Natl Acad Sci USA* 115:5762–5767.
- Nagel G, Ollig D, Fuhrmann M, Kateriya S, Musti AM, Bamberg E, Hegemann P (2002) Channelrhodopsin-1: a light-gated proton channel in green algae. *Science* 296:2395–2398.
- Nagel G, Szellas T, Huhn W, Kateriya S, Adeishvili N, Berthold P, Ollig D, Hegemann P, Bamberg E (2003) Channelrhodopsin-2, a directly light-gated cation-selective membrane channel. *Proc Natl Acad Sci USA* 100:13940–13945.
- Nam JH (2014) Microstructures in the organ of Corti help outer hair cells form traveling waves along the cochlear coil. *Biophys J* 106:2426–2433.
- Nenov AP, Chen C, Bobbin RP (1998) Outward rectifying potassium currents are the dominant voltage activated currents present in Deiters' cells. *Hear Res* 123:168–182.
- Parsa A, Webster P, Kalinec F (2012) Deiters cells tread a narrow path: the Deiters cells-basilar membrane junction. *Hear Res* 290:13–20.
- Ramamoorthy S, Nuttall AL (2012) Outer hair cell somatic electromotility in vivo and power transfer to the organ of Corti. *Biophys J* 102:388–398.
- Ren T, He W, Kemp D (2016) Reticular lamina and basilar membrane vibrations in living mouse cochlea. *Proc Natl Acad Sci USA* 113:9910–9915.
- Robles L, Ruggero MA (2001) Mechanics of the mammalian cochlea. *Physiol Rev* 81:1305–1352.
- Russell IJ (1983) Origin of the receptor potential in inner hair cells of the mammalian cochlea: evidence for Davis' theory. *Nature* 301:334–336.
- Russell IJ, Kössl M (1992a) Sensory transduction and frequency selectivity in the basal turn of the guinea-pig cochlea. *Philos Trans R Soc Lond B Biol Sci* 336:317–324.
- Russell IJ, Kössl M (1992b) Modulation of hair cell voltage responses to tones by low-frequency biasing of the basilar membrane in the guinea pig cochlea. *J Neurosci* 12:1587–1601.
- Russell IJ, Cody AR, Richardson GP (1986) The responses of inner and outer hair cells in the basal turn of the guinea-pig cochlea and in the mouse cochlea grown in vitro. *Hear Res* 22:199–216.
- Russell IJ, Kössl M, Murugasu E (1995) A comparison between tone-evoked voltage responses of hair cells and basilar membrane displacements recorded in the basal turn of the guinea pig cochlea. In: *Advances in hearing research* (Manley GA, Klump GM, Köppl C, Fastl H, Oeckinghaus H, eds), pp 136–144. Singapore: World Scientific.
- Santos-Sacchi J (1985) The effects of cytoplasmic acidification upon electrical coupling in the organ of Corti. *Hear Res* 19:207–215.
- Santos-Sacchi J (1986) Dye coupling in the organ of Corti. *Cell Tissue Res* 245:525–529.
- Santos-Sacchi J (1991) Isolated supporting cells from the organ of Corti: some whole cell electrical characteristics and estimates of gap junctional conductance. *Hear Res* 52:89–98.
- Santos-Sacchi J, Dilger JP (1988) Whole cell currents and mechanical responses of isolated outer hair cells. *Hear Res* 35:143–150.
- Soons JA, Ricci AJ, Steele CR, Puria S (2015) Cytoarchitecture of the mouse organ of Corti from base to apex, determined using in situ two-photon imaging. *J Assoc Res Otolaryngol* 16:47–66.
- Walters BJ, Coak E, Dearman J, Bailey G, Yamashita T, Kuo B, Zuo J (2017) In vivo interplay between p27Kip1, GATA3, ATOH1, and POU4F3 converts non-sensory cells to hair cells in adult mice. *Cell Rep* 19:307–320.
- Wang H, Wang S, Lu Y, Chen Y, Huang W, Qiu M, Wu H, Hua Y (2021) Cytoarchitecture and innervation of the mouse cochlear amplifier revealed by large-scale volume electron microscopy. *J Comp Neurol* 529:2958–2969.
- Wangemann P (2006) Supporting sensory transduction: cochlear fluid homeostasis and the endocochlear potential. *J Physiol* 576:11–21.
- Wu Y, Ramamoorthy S, Wilson T, Chen F, Porsov E, Subhash H, Foster S, Zhang Y, Omelchenko I, Bateschell M, Wang L, Brigande JV, Jiang ZG, Mao T, Nuttall AL (2016) Optogenetic control of mouse outer hair cells. *Biophys J* 110:493–502.
- Yu N, Zhao HB (2009) Modulation of outer hair cell electromotility by cochlear supporting cells and gap junctions. *PLoS One* 4:e7923.
- Zhang F, Wang LP, Brauner M, Liewald JF, Kay K, Watzke N, Wood PG, Bamberg E, Nagel G, Gottschalk A, Deisseroth K (2007) Multimodal fast optical interrogation of neural circuitry. *Nature* 446:633–639.
- Zdebek AA, Wangemann P, Jentsch TJ (2009) Potassium ion movement in the inner ear: insights from genetic disease and mouse models. *Physiology (Bethesda)* 24:307–316.
- Zhu Y, Liang C, Chen J, Zong L, Chen GD, Zhao HB (2013) Active cochlear amplification is dependent on supporting cell gap junctions. *Nat Commun* 4:1–8.